Pressure Effects on the Ensemble Dynamics of Ubiquitin Inspected with Molecular Dynamics Simulations and Isotropic Reorientational Eigenmode Dynamics

Nikolaos G. Sgourakis,*† Ryan Day,†‡ Scott A. McCallum,*† and Angel E. Garcia†‡
*Department of Biology, †Center for Biotechnology and Interdisciplinary Studies, and ‡Department of Physics and Applied Physics and Astronomy, Rensselaer Polytechnic Institute, Troy, New York

ABSTRACT According to NMR chemical shift data, the ensemble of ubiquitin is a mixture of "open" and "closed" conformations at rapid equilibrium. Pressure perturbations provide the means to study the transition between the two conformers by imposing an additional constraint on the system's partial molar volume. Here we use nanosecond-timescale molecular dynamics simulations to characterize the network of correlated motions accessible to the conformers at low- and high-pressure conditions. Using the isotropic reorientational eigenmode dynamics formalism to analyze our simulation trajectories, we reproduce NMR relaxation data without fitting any parameters of our model. Comparative analysis of our results suggests that the two conformations behave very differently. The dynamics of the "closed" conformation are almost unaffected by pressure and are dominated by large-amplitude correlated motions of residues 23–34 in the extended α-helix. The "open" conformation under conditions of normal pressure displays increased mobility, focused on the loop residues 17–20, 46–55, and 58–59 at the bottom of the core of the structure, as well as the C-terminal residues 69–76, that directly participate in key protein-protein interactions. For the same conformation, a pressure increase induces a loss of separability between molecular tumbling and internal dynamics, while motions between different backbone sites become uncorrelated.

INTRODUCTION

Ubiquitin is a well-studied protein of eukaryotic cells (1). This 76-residue-long protein participates in several important cell processes, such as the cell cycle, signal transduction, and cell death. A very important aspect of ubiquitin's function is to control the selective degradation of cellular proteins: a covalent linkage with several ubiquitin subunits is the signal that targets a protein for degradation by the proteasome, a highly conserved multisubunit protein complex (2). Ubiquitin's structural features have been investigated in studies using x-ray crystallography and solution NMR (3–6), all of which consistently report a mixed α/β structure with a well-packed core and a flexible C-terminus. The global diffusion properties, internal motions, and conformational dynamics of ubiquitin have also been investigated by NMR spectroscopy as well as molecular dynamics (MD) simulations in numerous studies (7–16).

The existence of multiple isoenergenic (to first approximation) conformations, known as conformational substates or conformers, in the energy landscape of proteins was first described by Frauenfelder and co-workers (17). In a recent study, Kitahara and co-workers (18) revealed the degree of structural variability within ubiquitin's conformational ensemble by using the online variable pressure cell NMR technique developed by their group. Variable pressure conditions offer the unique opportunity to experimentally alter the relative populations within a protein's conformational ensemble through the stabilization of the system's configurations that minimize total volume. That study reported two major conformer populations: N1 and N2. N1 is the ''closed'' form, which has a larger partial molar volume and dominates the ensemble at low-pressure conditions. At higher pressure, the N2 ''open'' conformer becomes the dominant population of the ensemble. The structures of the two conformers were determined at atomic resolution in a subsequent study by the same group (19), which demonstrated that N2 displays a more flexible C-terminus, a partially hydrated core, a perturbed hydrogen bond network involving the strand β_5, and a 9° tilt in the angle of the extended α-helix (residues 23–34) relative to the low-pressure structure. In the same study, the authors also measured NMR ^{15}N relaxation rate constants as a probe of ubiquitin's internal dynamics, under conditions of low (30 bar) and high (3 kbar) pressure (19). However, despite these large-amplitude fluctuations in the structure of the two populations, a model-free analysis of the NMR data failed to identify any significant differences in the dynamics among the low- and high-pressure ensembles. In this study we address the issue of dynamic variability between the two dominant conformers of ubiquitin's ensemble. Our results suggest that the large structural changes associated with the transition from N1 to N2 are accommodated by distinct differences in backbone dynamics that are not evident by the model-free interpretation of the NMR relaxation rate constants in Kitahara et al. (19). Furthermore, we propose that the pressure increase results in significant changes in the correlated dynamics of the system.

Protein dynamics are considered an inseparable attribute of protein structure that contribute to protein stability and

Submitted March 17, 2008, and accepted for publication May 22, 2008.

Address reprint requests to Angel E. Garcia, E-mail: angel@rpi.edu.

Editor: Kathleen B. Hall.

0006-3495/08/10/3943/13 $2.00

doi: 10.1529/biophysj.108.133702

function. NMR relaxation rate constants contain information on the range of motions accessible to proteins on the picosecond-nanosecond timescale. However, their interpretation is usually hampered by the assumption of separability between global tumbling and internal motions. The distinct modeling of global tumbling and internal motions is best represented by the popular model-free analysis, in which NMR relaxation constants are used to fit a generalized order parameter that measures the degree of spatial restriction of the motion, and an effective correlation time that is a measure of the rate of the motion (20). This assumption does not adequately describe flexible parts of proteins, or systems with large fluctuations in their conformational ensemble. NMR relaxation rate constants can contain contributions from different ensemble populations that display distinct structural features with amplitude-modulated motions; therefore, their interpretation on the basis of a simple model or a set of mobility parameters is, for these cases, incomplete (21).

In the case of a fluctuating protein structure, such as the current view of ubiquitin's ensemble, the lack of an overall alignment frame impedes the separation of the internal motional contribution from the global diffusion of the system as a whole. Thus, interpretation of NMR relaxation data on the basis of common analytical models, such as the standard model-free approach (20,22) or its derivative, the extended model-free approach (23), results in systematic errors since the contribution of global diffusion to the generalized order parameter is nonnegligible. Consequently, the model-free derived order parameters are expected to represent a biased estimate of the systems internal motions (24). The use of MD simulations to predict/interpret NMR relaxation rates is an attractive alternative to standard analytical models (25–27). However, due to inadequate sampling of global diffusion during the MD trajectory lengths accessible in simulations (nanosecond timescale), the calculation of relaxation parameters directly from the MD simulation data is prone to a nonnegligible amount of statistical error. In the case of disordered proteins, the lack of an overall alignment frame further impedes the calculation of NMR order parameters from long MD trajectories.

To overcome these inherent limitations in the analysis of relaxation constants, Prompers and Bruschweiller (28) developed a rather elegant and robust approach, called the isotropic reorientational eigenmode dynamics (iRED) method. This method is a novel way to interpret and relate NMR relaxation data with results from MD simulations to obtain an accurate description of protein dynamics. iRED is based on the calculation of a covariance matrix of the interactions under consideration, expressed as the Legendre polynomial of the angle between the bond vectors (sites). The matrix is averaged throughout the simulation, while its diagonalization yields the principal modes of concerted motions in the protein (eigenvectors) and their corresponding collective amplitudes (eigenvalues). The resulting eigenmodes may include contributions from both global tumbling and internal motions. This overcomes the need for an overall alignment frame, a condition not met for long MD trajectories, especially in the case of disordered proteins. As shown in the original description of the iRED method, relaxation parameters can be efficiently computed from MD trajectories on the nanosecond timescale by analytically integrating each snapshot over an isotropic distribution of directions. More importantly, like its predecessor RED (29), iRED can directly interpret relaxation data and detect concerted motions on the basis of groups of residues, rather than on a residue-by-residue basis, as provided by the model-free formalism. This allows the derivation of correlations between residues in terms of their dynamics, a conclusion not apparent by a simple inspection of the structure (30), or the model-free derived order parameters. In the case of a stable, well-folded protein molecule, the contribution from five large-amplitude eigenmodes dominates the system's global dynamics. Consequently, in this limit the model-free derived order parameter would be equivalent to that calculated with iRED by summing over all contributions from internal modes. iRED and RED previously have been applied to characterize the dynamics of ubiquitin in the native and partially folded ''A-state'', which is observed in aqueous alcohol solutions conditions of low dielectric constant and pH (28,31), the iron-responsive element (IRE) RNA hairpin (32), the complex of the U1 snRNA with its protein partner RDB1 (33), and the HIV-1 transactivation response RNA element (TAR) (34).

In this study, we used nanosecond-timescale MD simulations and the iRED formalism to investigate the range of dynamical changes within the two dominant conformers of ubiquitin, N1 and N2, under conditions of high and low pressure. A pressure increase provides the means to study the consequence of water penetration inside the core of the protein and the stabilization of lower volume configurations of the system on its dynamics (35). We used backbone amides as probes of ubiquitin's dynamics and correlated our results with experimentally measured longitudinal ^{15}N relaxation rate constants provided by Kitahara and co-workers (19). Averaging of the relaxation rate constants, as calculated with iRED for individual trajectories, produces the final ensemble-averaged relaxation rate constants. When compared with the previously published NMR data (19), the iRED results show good agreement. However, although these changes in dynamics induced by increased pressure were not appreciated by the model-free analysis of Kitahara et al. (19), our results suggest that the two conformers behave very differently. The dynamical changes associated with the increase in pressure and the consequent transition from N1 to N2 can be attributed to the correlated motions of several residues located on the extended α-helix 23–34, the loop region 46–55, and the C-terminus. These regions are crucial for ubiquitin's function because they participate in the binding site of interacting protein partners. Furthermore, a detailed analysis of our results suggests that pressure has very different effects on the dynamics of the two conformers: pressure increase has a

moderate effect in the dynamics of N1, whereas for N2 high pressure results in the loss of separability of internal and global motions, and a decrease in the extent of sequence correlations in internal dynamics, a feature that is indicative of a less structured system.

MATERIALS AND METHODS

MD simulations

Simulations were run in either AMBER 8 (36) or GROMACS 3.3 (37) using the Amber94 force field (38) and TIP3P water model (39). The 30 bar (N1) (Protein Data Bank (PDB) id: 1V80) and 3000 bar (N2) (PDB id: 1V81) NMR ensembles consist of 10 structures each (19). We selected the most representative conformation of the high- and low-pressure NMR ensembles according to the annotation found in the aforementioned PDB files. For the N2 ensemble, we simulated one additional conformation to verify the separability results. These conformations were used as starting points for 10-ns-long MD simulations at 300 K and 1 atm. The configurations after 5 ns of these simulations were used as starting points for 10–20-ns simulations at 300 K and 3000 atm. Each conformation was solvated in 8959 water molecules and 11 Na^+ and 11 Cl^- ions, giving one counterion for each charged amino acid in the protein. Temperature was controlled using a Nosé-Hoover thermostat with a 5-ps coupling time (40,41) and pressure was controlled using a Parinello-Rahman barostat with a 5-ps coupling time (42). The protein and solvent were coupled to independent temperature baths. The system compressibility was set to 4.6×10^{-5} bar^{-1} for simulations at 1 atm, 2.3×10^{-5} bar^{-1} for simulations at 3000 atm, and 1.4×10^{-5} bar^{-1} for simulations at 6000 atm, corresponding to experimentally determined water compressibilities (http://webbook.nist.gov). Long-range electrostatic interactions were calculated using particle-mesh Ewald (43) with a grid spacing of 1.2 Å and cubic interpolation. Van der Waals energies were cut off at 10 Å. A 2-fs time step was used and the nonbonded list was updated every 10 integration steps.

iRED analysis

The iRED formalism was used to analyze the dynamics of both conformers based on the high- and low-pressure MD trajectories. iRED is based on the calculation of a real, symmetric covariance matrix M for n interactions (sites). The elements of the covariance matrix are the second-order Legendre polynomials of the angle between each pair of amide bond vectors. The matrix is ensemble-averaged throughout the MD trajectory and diagonalized to yield the reorientational modes $|m\rangle$ and the corresponding eigenvalues λ_m. The eigenvectors contain information on the contribution of each mode to the dynamics of different sites, whereas the eigenvalues quantify the amplitude of each mode. Under the assumption of separability between internal and global motions, the Lipari-Szabo order parameter for site i can be calculated as a sum of the contribution of all ''internal'' modes:

$$1 - S_i^2 = \sum_{6}^{n} \delta S_{m,i}^2,$$

where, in the case of a well-folded protein, the five largest modes that correspond to global tumbling are not included in the summation.

The individual components δS^2 are calculated in a preceding step as

$$\delta S_{m,i}^2 = \lambda_m |\langle m|M|i\rangle|^2,$$

where M is the covariance matrix in its eigenbasis, m is the mode under consideration, and i is the residue index.

As a measure of correlation between the dynamics of sites i and j, we calculated the expression

$$Cor_{i,j} = \lambda_m \cdot \langle m_i^{2T} | m_j^{2T} \rangle,$$

where m^{2T} is the transpose of the diagonalized covariance matrix m, with its elements squared. Values of this correlation index were calculated for each pair of sites and plotted in contour maps (see Fig. 6) to illustrate the correlations in dynamic behavior along the sequence of ubiquitin. This measure is not dependent on the separability assumption, since it contains contributions from all modes.

To calculate NMR relaxation parameters, time decay information must be extracted from the simulation trajectories. This is done by calculating the projections of all rank 2 spherical harmonics for each interaction on the previously described eigenvectors:

$$\langle Y_{2,m} | m \rangle (t),$$

where the subscript m in the spherical harmonic can take values from $-2 \ldots 2$.

Time correlation functions of the projected spherical harmonics can then be ensemble-averaged throughout the trajectory. The total correlation function for mode m is given by:

$$Ctot_m(t) = \sum_{m=-2}^{2} \overline{\langle Y_{2,m} | m \rangle (\tau) \cdot \langle Y_{2,m} | m \rangle^* (\tau + t)}.$$

We used the last 9 ns of all 10-ns-long trajectories to calculate the NMR relaxation data (Table 1). Most spherical harmonics were found to decay monoexponentially in good approximation with correlation time constants at the subnanosecond regime. The fitted correlation times were used to calculate the spectral density function analytically, as previously described (29). The longitudinal relaxation rate $R1$ can then be calculated directly from the spectral density function, according to relaxation theory (44). In this calculation, we used a chemical shift anistotropy (CSA) of -176 ppm for the ^{15}N spin and a value of 1.04 A for the average length of the amide bond, as suggested in the original iRED publication. Calculations were carried out for an external magnetic field of 18.79 T (equivalent to a ^{15}N Larmor frequency of 81.1 MHz).

We used the χ^2 as a measure of proximity to the experimentally determined $R1$ values:

$$\chi^2 = \sum_i \frac{(R1_{iRED} - R1_{NMR})^2}{\sigma_{NMR}^2}.$$

This estimate was used to fit the ratio of the populations of the two conformers in both high- and low-pressure ensembles, and to assess the

TABLE 1 Comparison with experimental data

Pressure	starting conformer	error 1	error 2	error 3
3 bar/1 atm	N1	1668	1310	1097
	N2	2496		
3 kbar/3 atm	N1	2647	1836	1184
	N2	1776		

The χ^2 error (computed as described in Materials and Methods) was used to assess the validity of our simulation trajectories, based on the calculated longitudinal relaxation rate constants. $R1$ constants were calculated with the iRED method (29) based on an isotropic distribution of molecular orientations with respect to the laboratory frame. Experimental values were measured by Kitahara and co-workers (19) at 3 bar and 3 kbar pressure conditions. Results from individual trajectories, starting from the N1 and N2 conformers under conditions of low and high pressure (1 atm and 3000 atm, respectively), are compared directly with the experimental values that were obtained under conditions of similar pressure (error 1), or are averaged to produce the final, ensemble-averaged relaxation rate constants. The ratio of the two populations was adapted from a fitting of chemical shift data (19) (error 2) or according to a least-squares fitting of the $R1$ constants, as described in Materials and Methods (error 3).

validity of our simulation trajectories. For the low-pressure trajectories, the ratio of populations for the two conformers that minimized the error was found to be N1:N2 57:43. At high pressure, the fitted ratio was 48:52. In contrast to the original iRED publication, no additional fitting of correlation times τ_m was required to reproduce the experimental data.

RESULTS

Inspection of overall dynamical behavior

The eigenmode collectivity plot (i.e., the fraction of amide bond vectors that participate in a given correlated motion, κ) versus the eigenvalues of the mode (λ) provides a summary of the motions accessible to each system (defined in Prompers and Bruschweiler (28)). When expressed on a log x scale, it provides a ''fingerprint'' of all correlated motions with the peptides. For an ideally rigid molecule with no internal motions, this plot should only contain five points with nonzero λ, since diagonalization of the covariance matrix would yield only five nonzero eigenvalues. For systems with some correlated internal motions, we would expect the modes that correspond to the internal motions to appear at lower (λ, κ) values, resulting in a large separation (gap) from the five larger (λ, κ) points. The corresponding plots for our MD simulations of ubiquitin demonstrate clear differences in the pressure dependence of the dynamics of the two conformers. At low pressure (Fig. 1, *a* and *c*), both conformers display separability between internal motions and global tumbling, as indicated by a large gap in the λ dimension. The gap is larger for the N1 conformer, which indicates a behavior that resembles an ideally folded protein with rapid internal motions for the low-pressure dominant population, under conditions of low pressure. The degree of separability between global and internal modes can be further quantified by a separability index of 4.50 and 3.70 for N1 and N2, respectively. In the limiting case of a static structure, the separability index is infinite (for a definition of the separability index, see Prompers and Bruschweiler (28)). However, at high pressure the conformer N1 retains separability, whereas N2 diverges from the typical behavior of a well-folded system. This loss of separability is clearly apparent in the κ versus λ plot for the N2 conformer, since a more widely scattered distribution of modes is observed with no clear gap between the five overall modes from the remaining, more local-oriented modes (Fig. 1 *d*). The separability indices for the two conformers at high pressure further illustrate this trend, with values of 4.56 and 2.78, respectively. In the case of the N2 conformer under conditions of high pressure, the separability index is closer to that of a less ordered system, as measured in previous iRED studies (28).

Generalized order parameters

A direct comparison of the order parameter derived with model-free analysis based on the NMR relaxation data (19) with the results of the iRED analysis of our MD trajectories is shown in Fig. 2. In general, we observe good agreement with the model-free order parameter under conditions of low pressure. However, at residues 7–13, 17–20, 46–50, 56–58, 60–61, 65—66, and 72 the model-free derived order parameters are significantly higher than those calculated with iRED, particularly for the N2 conformer. The model-free formalism (20,22) may inadequately describe the dynamic character of these regions, which are found to be poorly restrained in the NMR structures. Furthermore, these regions

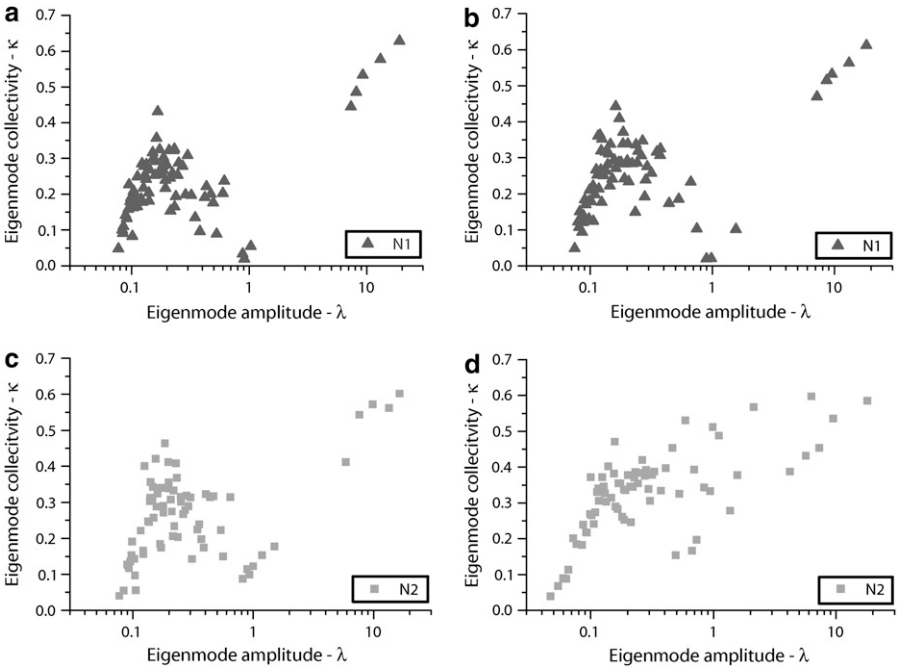

FIGURE 1 Eigenmode collectivity plots. The eigenmode collectivity κ (i.e., fraction of sites significantly affected by the mode) is plotted versus the amplitude of the mode λ, which is quantified by the eigenvalue of the mode. This summarizes the range and properties of the system's dynamics. Calculations derived from the N1 and N2 conformer trajectories are plotted as triangles and squares, respectively. (*a* and *c*) Low-pressure simulation trajectories: both conformers display separability between internal motions and global tumbling. (*b* and *d*) High-pressure simulation trajectories: the N2 conformer loses separability as internal motions intermingle with global tumbling to result in overall reorientational modes.

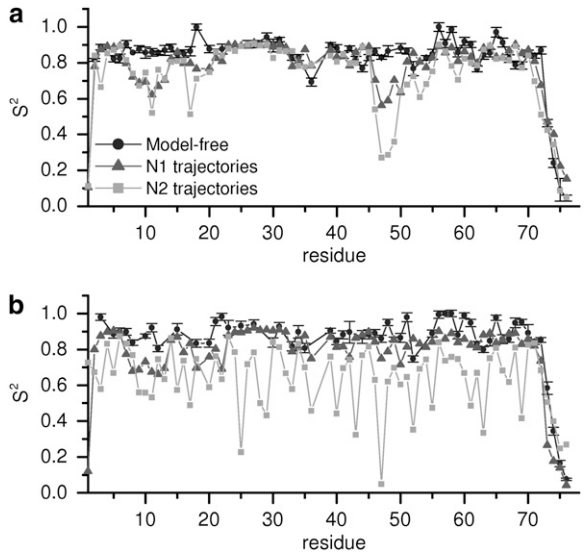

FIGURE 2 Comparison of the generalized order parameters. The calculated order parameters are plotted together with the fitted order parameters from standard model-free analysis of the NMR relaxation data (19). Fitted parameters are shown with circles; calculations derived from the N1 and N2 conformer trajectories are shown as triangles and squares, respectively. (*a*) Low-pressure simulations and experiments. (*b*) High-pressure results. We observe the inefficiency of the order parameter for the N2 trajectory to account for the system's dynamics at high pressure, as a result of the breakdown of separability between internal motions and global tumbling of the protein.

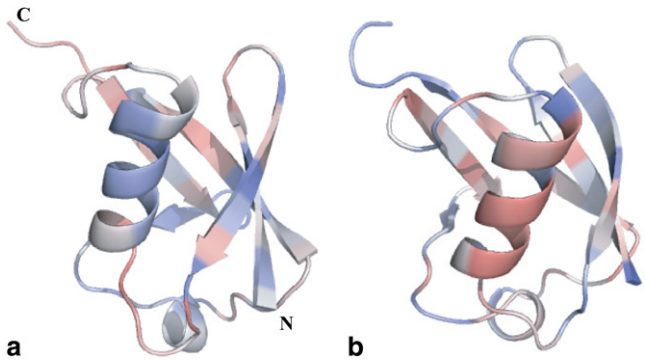

FIGURE 3 Pressure effects in the dynamics of the dominant conformers N1 and N2. Pressure-induced changes in the order parameter are illustrated on the structure of each dominant conformer. The amide bond vectors are used as probes of internal dynamics. Order parameters were calculated from our MD trajectories based on an iRED analysis of rank 2. Red and blue respectively denote smaller and larger order parameters at high-pressure (3000 atm) relative to low-pressure (1 atm) trajectories, indicating increased and reduced mobility, respectively. We observe small changes in dynamics for the N1 conformer (*a*) at different pressure conditions. For the N2 conformer (*b*) the pressure increase induces dramatic changes in the system's overall dynamics. Secondary structure assignments in ribbon diagrams were adapted from Kitahara et al. (19) (PDB codes 1V80 and 1V81). Graphics were made with the visualization suite PyMOL (www.pymol.org).

are likely to undergo conformational exchange on a much slower timescale (μs-ms) than the one probed by the generalized order parameter (ps-ns). This concern is supported by the exchange contributions to the ^{15}N transverse relaxation rate constants measured by Kitahara et al. (19). Specifically, the region 46–50 is contained within a large loop, including a short 3_{10} helix with few restraints from tertiary interactions, wheas high exchange rate constants (of a few 10 s^{-1}) were observed for residues 21–44 and 70. Chemical exchange is expected to have a nonnegligible contribution to the transverse relaxation rate constants R2, which are used to fit the model-free order parameters. These motions occur in the microsecond to millisecond timescale, a fact that contradicts the basic assumption of the model-free formalism (i.e., $\omega\tau_i < 0.5$, where ω is the Larmor frequency of ^{15}N, and τ_i is the effective correlation time of the internal motions). In addition, another basic assumption of the model-free approach, i.e., the separability between global and internal motions, is not expected to hold for these regions due to their participation in large-amplitude structural fluctuations (19); therefore, the model-free order parameter is expected to be a biased estimate of the system's internal motions (28).

In Fig. 3, changes in the system's dynamics as a result of pressure increase are illustrated on the structure of the two conformers. As anticipated by the collectivity plots, the N1 conformer displays a similar dynamical picture at high and low pressure based on the generalized order parameter (Fig. 2, *a* and *b*). The few residues with a pressure dependence of the order parameter are L8, E18, T22, and the segment 46–50. Residues E18 and T22 are located at the bottom of ubiquitin's core. E18 is found in the extended loop region, and T22 is adjacent to the extended α-helix. These two regions are found to have a lower-order parameter at high pressure, indicating a higher degree of mobility. On the other hand, the region 46–55 is found to have decreased flexibility at high pressure and is located within an extended loop spanning residues 44–66. In addition, the N1 conformer trajectories indicate that pressure increase induces a large increase in the mobility of the C-terminus and reduces the flexibility of the N-terminus.

The N2 conformer is more dynamic than N1 at several positions (Fig. 2 *a*). In particular, the entire loop-β-loop motif 46–55, the short 3_{10}-helix 58–59, and the C-terminus 69–76 are found to be more flexible in the N2 low-pressure ensemble with respect to N1. As previously shown, the position of the loop is affected by the conformational change associated with the transition from the N1 conformer to N2: the 9° tilt of the extended α-helix toward the N-terminal of the sequence results in bringing the extended loop 44–66 at a more central position with respect to the β-sheet (19). In addition, residues 3, 11, and 17 located at the first two β-strands are more flexible in N2 compared to N1, according to the iRED-derived order parameters.

At high pressure, the model-free derived generalized order parameters for the N2 conformer fail to account for the internal motions of the system, as observed in our MD simulations (Fig. 2 *b*). This is anticipated by the low separability index for this ensemble. At 3000 atm, N2 behaves like a

disordered system, according to the separability plots of Fig. 1 *d*. Therefore, the order parameter contains contributions from global tumbling in addition to internal reorientational modes. An inspection of the range of dynamical changes on the structure conformation (Fig. 3 *b*) reveals the increased mobility of the extended helix at high pressure, and decreased mobility of the N-terminus.

Comparison of correlated motions

For the N1 conformer, the largest amplitude mode involves residues 23–34, which span the entire length of the extended α-helix (Fig. 4 *a*). Residues 6, 42, 44, 50, 55, and 68 are also affected to a large extended by this reorientational mode (contribution of >50%). These residues are located on the interaction surface along the core β-sheet that opposes the extended α-helix. The participation of several residues distributed along the sequence of ubiquitin indicates that this is indeed a global mode that corresponds to a motion of the helix relative to the β-sheet. This motion may reflect an initial step in opening and closing of the core of the structure. At higher pressure, T55 is also affected by this mode (contribution of ~55%). This residue is located on a loop that is in close proximity to the N-terminal T22 adjacent to the α-helix. Notably, the relative position of these residues is altered in the high-pressure ensemble.

The second-largest mode affects a number of residues scattered throughout the entire sequence of ubiquitin (Fig. 4 *b*). However, the absence of any contribution to the motions of residues in the extended α-helix is striking. A cluster of residues affected by this mode is located at the β-sheet (residues 3, 4, 6, 10, 14, 66, and 67, contributions of >20% to the overall dynamics of these sites). Most of these residues are not significantly affected by the first mode, which indicates that this is indeed a separate mode with global character since it demonstrates a large collectivity index of 58% (i.e., the

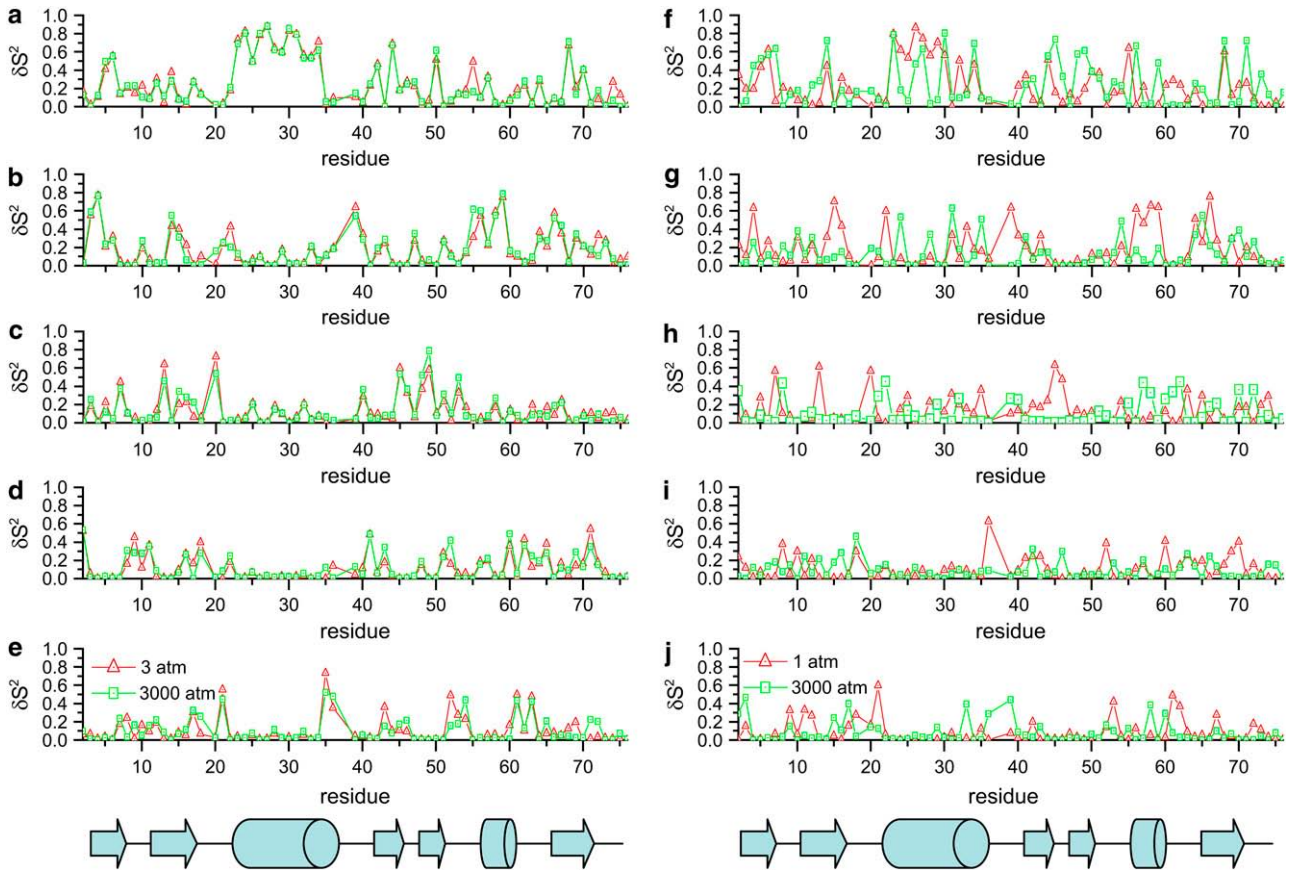

FIGURE 4 Correlated motions for the N1 and N2 ensembles. The values of the projections along the five principal eigenvectors δS^2 are shown here along the sequence of ubiquitin for the N1 (*a–e*) and N2 (*f–j*) conformer trajectories, at low (*triangles*) and high (*squares*) pressure conditions. At low-pressure conditions, projections on the remaining 68 eigenvectors constitute minor contributions to the system's dynamics and are not presented here. Proline residues are excluded from this analysis because they lack amide hydrogen atoms. For this conformer, we observe minor differences in correlated motions between the low- and high-pressure trajectories. Large changes in correlated motions accommodate the increase in pressure for the N2 conformer as a result of the loss of separability between internal dynamics and global tumbling of the system. Contributions from the remaining eigenmodes become significant descriptors of the system's dynamics at high pressure. The position of strands (*rectangles*) and helices (*cylinders*) is displayed in the inset for illustrative purposes. For a full description of correlated dynamics, please see text.

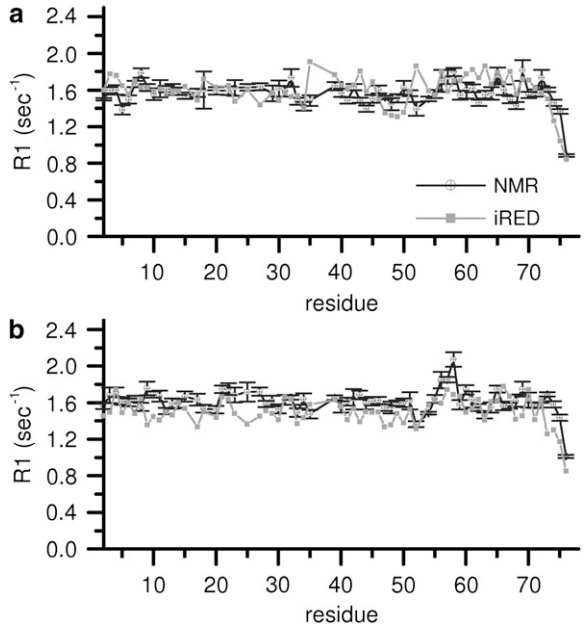

FIGURE 5 Ensemble-level comparisons with NMR experimental data. MD-derived and experimental longitudinal relaxation rate constants $R1$ are plotted for conditions of (*a*) low and (*b*) high pressure. $R1$ constants that were calculated from our simulation trajectories using the iRED formalism (*squares*) are in good agreement with the experimentally measured values from NMR relaxation experiments (*circles*) (19). A least-squares fitting procedure was used to determine the ratio of the contributions from the N1 and N2 populations in the final ensemble to be 57:43 for the low-pressure trajectories and 48:52 for the high-pressure trajectories. The ensemble-averaged calculations have a moderate χ^2 error on the order of 10^3 (1097 and 1184 for the low- and high-pressure ensembles, respectively).

dynamics of 42 out of 73 sites are significantly affected by this mode). The contributions of mode 2 to the dynamics of different sites are not altered at high pressure for the same conformer, with the exception of T22 (Fig. 4 *c*).

The third collective reorientational mode involves F45 and Q49, located at the loop-strand motif at the bottom of the structure. Residues T7, I13 and S20, located in end of the β_1-strand, the middle of the second β-strand and at the second loop also participate in this motion (contribution >40%). Residues E49 and G53, which are located within the extended loop region, are significantly more affected by this mode at higher pressure (78% and 50%, respectively).

The mode with the fourth-largest amplitude also affects residues throughout the sequence of ubiquitin. At low pressure, for the same conformer (N1), it contributes significantly (>30%) to the dynamics of loop residues 2, 10, 11, 18, 41, 51, 60, 62, 65, and 71. L43, D52, and N60 become increasingly affected by mode 4 at higher pressure conditions. The fifth mode is, again, an overall reorientational mode, with significant contributions to the dynamics of 44% of all sites. This mode also contributes significantly (>50%) to the dynamics of the short loop motif ^{35}GIP^{38}P that follows the extended α-helix, and this contribution is larger at lower pressure. L43, found at the short strand adjacent to the helix, is also affected by this mode.

The remaining modes represent highly localized motions that include clusters of 1–4 residues, as shown by the projections on the iRED eigenvectors (data not show). In general, we observe large contributions for some of these modes to the dynamics of the termini that correspond to sequence-specific motions with no global contribution.

At low pressure, the N2 conformer presents a picture very similar to that of the N1 conformer. Five large-amplitude, highly collective modes dominate the dynamics of the system, with the remaining modes to have small, localized contributions to the protein's internal dynamics (Fig. 4, *f–j*). Correlations in the motion of the amide bond vectors in the extended helix (residues 23–34) are also present at low pressure; however, the C-terminal residues of the helix at positions 31–34 are less affected by this mode (Fig. 4 *f*), compared to the N1 conformer. The remaining principal modes 2–5 show a very similar sequence profile as described for the N1 conformer, at low pressure. A striking exception involves the short loop motif ^{35}GPPP^{39}D. The contribution of mode 5 to the dynamics of this region is much smaller for the N2 conformer at low pressure, resulting in reduced flexibility (Fig. 4 *j*).

At increased pressure, lower modes also become significant determinants of the system's dynamics. On the other hand, the contribution of the five principal modes is diminished (Fig. 4, *f–j*, squares). Consequently, the system's internal modes contain contributions from global reorientations of the molecule. As a result, the model-free order parameter would not be expected to accurately account for the internal dynamics of the system.

Comparison with NMR relaxation data

The iRED formalism also allows us to calculate NMR relaxation rate constants according to an isotropic distribution of molecular frames. We used the longitudinal relaxation rate constant as a benchmark for the validity of our simulation trajectories because it contains no contribution from chemical exchange processes. Chemical exchange was indeed observed by means of relaxation rate analysis for several residues of ubiquitin at both low- and high-pressure ensembles (19). At each pressure, we used the iRED results derived from the individual trajectories of both conformers to calculate the ensemble averaged experimental observable. The ratio of the two conformers was optimized according to a least-squares fitting procedure. This ratio was found to be different at 1 atm and 3000 atm (N1:N2 57:43 for the low-pressure ensemble and 48:52 for the high-pressure ensemble), demonstrating the prevalence of the N1 conformer at the low-pressure ensemble and N2 at the high-pressure ensemble. This analysis is not intended to accurately represent the true population ratio of the two conformers, but it clearly indicates a pressure-in-

duced shift in the state equilibrium of the ensemble toward system configurations that minimize total volume.

For most amides the $R1$ relaxation rate constants calculated with iRED are in good agreement with the experimental measurements (Fig. 5 and Table 1), reaching an overall χ^2 error of 1097 for the low-pressure and 1184 for the high-pressure ensemble. These calculations were performed with a population ratio fitted to reproduce the experimental results, as described in Materials and Methods. When we used the experimentally determined ratio of N1:N2 85:15 at 30 bar and 23:77 at 3 kbar (18), the ensemble-averaged calculation resulted in larger χ^2 errors of 1310 and 1836 in the final observable, as anticipated. Furthermore, we observe that for the individual trajectories, the agreement with experimental results is better when the pressure conditions match the starting conformer, such that the N1 1 atm trajectory is in better agreement with the low-pressure results, whereas the N2 3000 atm trajectory is in better agreement with the experimental results obtained at high-pressure conditions.

DISCUSSION

We have presented an integrated, ensemble-level description of ubiquitin's dynamics under conditions of high and low pressure. The implementation of pressure as a variable allows us to study the dynamical response of different conformers within ubiquitin's ensemble to a pressure increase. Our application of the iRED formalism allows the correlations in atomic motions along the different amide bond sites to be deduced. Furthermore, we are able to calculate NMR relaxation parameters from the 10-ns-long MD simulation trajectories. Our simulation calculations were found to be in good agreement with NMR experimental measurements reported by Kitahara et al. (19). However, our goal here is not to accurately reproduce experimental relaxation results, as these depend strongly on the correlation times of the global and internal reorientational modes. When they introduced the method, Bruschweiller and Prompers (28) showed that $R1$, $R2$, and the heteronuclear nuclear Overhauser effect (hNOE) can be effectively reproduced from the iRED covariance matrix by nonlinearly fitting the correlation times to the experimental data. In the study presented here, no fitting of parameters was used, other than the ratio of the two conformer populations in the final ensemble. Our results, in terms of the longitudinal relaxation rate constants $R1$, correlate with experiments with a precision comparable to that achieved in this initial report (28) and all subsequent iRED publications, according to the reported χ^2 error values (on the order of 10^3); however, this agreement does not extend to $R2$ and hnNOE (results in the Supplementary Material, Fig. S1, Fig. S2, Data S1). This is due to a nonnegligible statistical error that arises from the fitting of correlation functions, particularly those that correspond to contributions from global modes. As shown by Zwanzig and Ailawadi (45), the relative error in a time correlation function obtained by averaging over an MD trajectory with a window t is of order $1/\sqrt{t}$, in the case of a Gaussian random variable. Thus, in the case of global tumbling, which has been shown experimentally to have a time constant of ~4 ns (8,9), a sampling of 100 ns would be needed to obtain an accuracy on the order of 1%. This is beyond the scope of this study. Rather, our study aims to provide a plausible model of correlated motions and their pressure dependence in the context of the two conformers N1 and N2. Since the model emerges from the diagonalized covariance matrix, as shown in Materials and Methods, it is intuitive to assess the convergence of the resulting iRED eigenvectors. To perform that task, we calculated the dot products of the normalized eigenvectors that corresponded to the five larger reorientational modes obtained at different fractions of the 9-ns trajectories with those that were obtained over the entire trajectory length. The results shown in Fig. 7 indicate that the covariance matrix is well converged at the

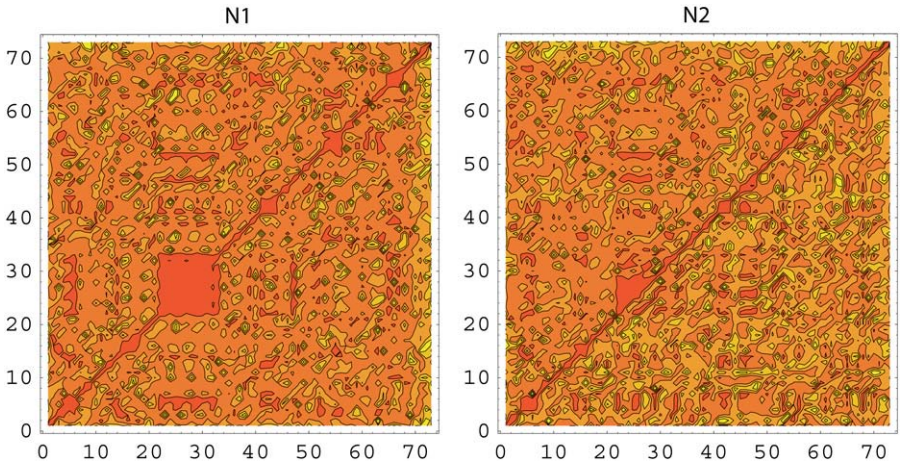

FIGURE 6 Correlated dynamics maps. Correlations in the motions of individual amide bond vectors are illustrated here for both conformers in low-pressure (1 atm) and high-pressure (3000 atm) simulations. We used the inner products of the transpose of the diagonalized covariance matrix multiplied by its eigenvalues as a measure of the degree of correlation in the motion of two vectors, as described in Materials and Methods. Contours are drawn according to a log scale; the red color denotes highly correlated dynamic behavior. Indexing of the amides disregards proline residues at positions 19, 37, and 38 of ubiquitin's sequence. The upper-left and lower-right quadrants of each map are calculated from low- and high-pressure simulation trajectories, respectively. We observe a low- to medium-range correlation in dynamics as a result of localized, internal motions, and long-range correlations as a result of global motions. For the N1 conformer, the off-diagonal high-density contour involving residues 23–34 corresponds to the extended α-helical segment. A decay of correlations in the amide bond dynamics for the N2 conformer is observed at high pressure.

10-ns timescale for the N1 conformer trajectories and the N2 low-pressure trajectories. Eigenvectors are essentially collinear after 4–5 ns of simulation time (the eigenvalues converge to their final values much more rapidly, after 1–2 ns). In fact, we observe that modes that correspond to global motions converge more rapidly, as anticipated from their larger amplitude and more collective character. Convergence of the iRED eigenvectors takes a longer time for the trajectories of the N2 conformer under conditions of high pressure. To investigate this, we extended this simulation to 20 ns of production time. The five largest amplitude eigenvectors converge at a much longer timescale of 10–12 ns (Fig. 7 *d*). Analysis of the iRED collectivity plots for the 20-ns-long trajectory indicates a behavior very similar to that observed in the first 10 ns, with a lack of a separability gap between the global and internal modes (results in the Supplementary Material, Fig. S1, Fig. S2, Data S1). This is a further indication that the dynamics of the system as represented by the diagonalized iRED covariance matrix are sufficiently described by 10-ns-long trajectories; however, the five principal modes are not a sufficient descriptor of the system's dynamics since contributions from large-amplitude internal modes affect the dynamics of the system significantly. Therefore, more eigenvectors are needed to provide a sufficient description of reorientational motions.

These calculations (as well as the calculations of order parameters) are prone to a small amount of systematic error that results from the classical treatment of the system in our MD simulations. A previous theoretical study based on normal modes derived from atomistic potentials for the crystal structure of the BPTI protein (46) indicated that high-frequency modes may contribute to the angular part of the order parameter and consequently affect the calculation of relaxation rate constants, resulting in an apparent increase of relative magnitude 5% with respect to results from a quantum treatment of the system.

In their pioneering NMR study, Kitahara and co-workers quantified the differential stabilization of the two dominant conformers, N1 and N2, in the final ensemble with pressure change based on fitting of NMR chemical shift data (18). In the study presented here, the prevalence of the N1 conformer population at low pressure and the N2 at high pressure emerges from the comparison of the calculated longitudinal relaxation rate constants with their experimentally determined values (Table 1). $R1$ relaxation values calculated for the N1 conformer are in significantly better agreement with the experimental results at low pressure, as shown by the corresponding χ^2 errors (1668 for the N1 trajectories versus 2496 for the N2 trajectories). At 3000 atm pressure, the picture is inverted, with the N2 trajectories being more consistent with the experimental ensemble according to this experimental observable (χ^2 of 1776 for N2 versus 2447 for N1). Optimizing this ratio according to least-square fitting to the relaxation data yields the correct experimental observation, i.e., that the N2 conformer is stabilized at sufficiently high pressure. Indeed, a least-squares fitting of the ratio yields a 57:43 prevalence of the N1 conformer at 1 atm pressure. At 3000 atm, the N2 conformer population is the dominant part of the ensemble, with a ratio of 48:52. Based on the NMR data of Kitahara and co-workers, it has been proposed that this effect is due to the smaller partial molar volume of the N2-dominated ensemble relative to N1 24 mL/

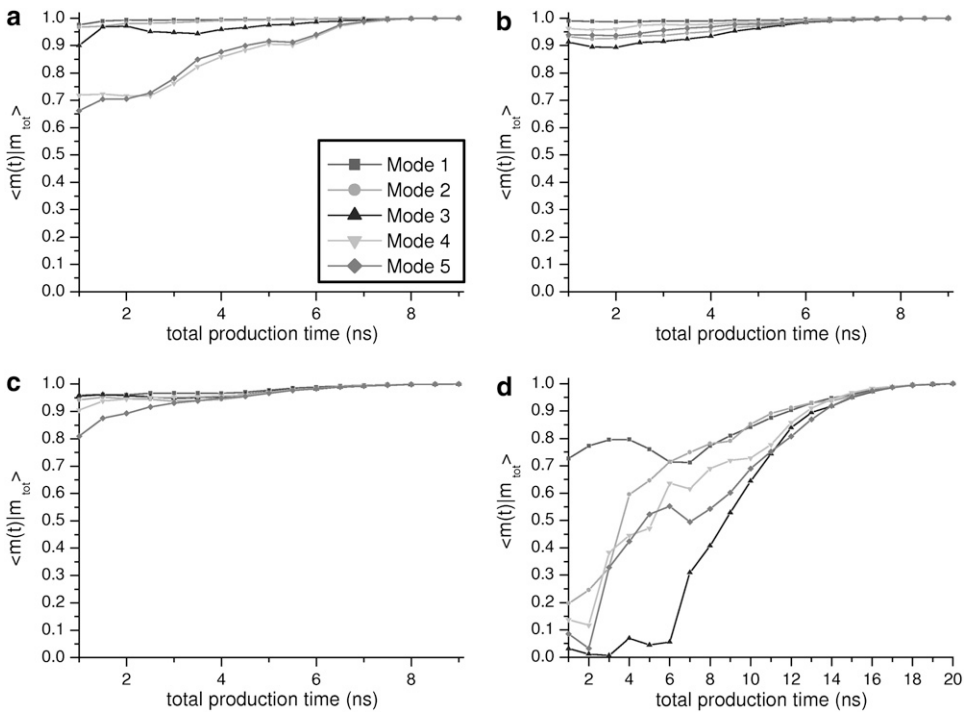

FIGURE 7 Convergence of iRED eigenvectors. The dot products of the iRED eigenvectors that correspond to the five largest in amplitude modes at different simulation times are used to assess the convergence of our MD-based models. The eigenvectors that were calculated from the entire production phase of the MD simulations (2–10 ns for both conformers at 1 atm and N1 at 3000 atm, and 2–21 ns for N2 at 3000 atm) were used as a reference. First row: trajectories starting from the N1 conformer under conditions of (*a*) low and (*b*) high pressure. Second row: trajectories starting from the N2 conformer under conditions of (*a*) low and (*b*) high pressure. See text for discussion on convergence.

mol (18). As shown in a recently published study by our group (11), this is because as a result of water penetration in the core of the protein, buried residues become solvated and experience a much lower volume under conditions of high pressure. The study presented here verifies these findings and suggests a concerted motional model associated with pressure increase. It should be noted that the changes in population ratios observed here are not as dramatic as those proposed by Kitahara et al. (18) based on NMR chemical shift data, where an 85:15 ratio at 30 bar is translated to a 23:77 proportion at 3000 bar. Although the simulation pressure conditions mimic the experimental ones (1 atm = 1.01325 bar), they are not identical. In addition, pressure effects are mediated, to a large extent, by the solvent, which is also a very important determinant of protein dynamics. Therefore, they are expected to be very sensitive to the choice of water model (in this study we used the TIP3P water model (39)). Assuming a two-state model for the two conformer populations, the differences in free energies between the calculated and measured relative populations are <4 kJ/mol, and smaller than the expected accuracy of our calculations.

It has been argued that the use of the TIP3P water model results in underestimation of the global correlation timescale by effectively ''speeding up'' the rotational diffusion. The effect emerges from the smaller apparent viscosity of TIP3P water in comparison to the experimental value (0.84 cp at 300 K and 1 atm). This behavior has been reported in two independent MD studies of pure TIP3P water, in which the calculated viscosity values were found to be 60.2% and 62%, respectively, of the experimental values that correspond to the simulation conditions (47,48). Shen and Freed (48) further demonstrated that the implementation of the Ewald summation method for the calculation of long-range electrostatics (43) in combination with the TIP3P water model results in an even larger deviation of the calculated viscosity from the experimental value (0.35 cP or 35% of the viscosity of real water). These observations corroborate the fact that the time constants calculated for ubiquitin in the original iRED publication were systematically lower than expected from experimentally determined overall tumbling correlation times (28). Indeed, a least-squares fitting of the five larger time constants based on experimentally determined relaxation parameters ($R1$, $R2$, and hnNOEs) resulted in an amplification by a factor of $\sim$10 (Table 1 in Prompers and Bruschweiler (28)). This effect was also manifested in our study by the fact that hnNOEs calculated with iRED from our simulation trajectories were found to also be systematically lower than the experimentally determined quantities (see the Supplementary Material, Fig. S1, Fig. S2, Data S1). Relaxation theory, supported by experimental evidence, reveals that hNOEs are very sensitive to internal motions and show a sigmoid dependence on the tumbling time constant (Fig. 2 in Kay et al. (49)). Therefore, the systematic error observed in our simulation trajectories could be due to the underestimation of the tumbling constant. Theoretical calculations based on hydrodynamic modeling of known structures of ubiquitin have shown that the rotational diffusion tensor is affected significantly by the extent of bound water, and are in best agreement with experimental data when half a water shell is considered (9). Taken together, these results suggest that the strength of protein-water interactions play an important role in the rotational behavior of proteins, and indicate a point for further improvement of current water models for use in modern simulation setups under the Ewald summation method, as first suggested by Feller et al. (47).

Pressure effects dramatically affect the dynamics of the N2 conformer, as suggested by our analysis. The loss of separability between internal dynamics and global tumbling is evidenced by the iRED ''fingerprint'' plots of Eigenmode collectivity versus amplitude. To assess whether our results for the N2 conformer depend on the choice of starting configuration from the published NMR ensemble, we also performed simulations starting from another conformation of the published NMR ensemble (PDB code 1V81, conformer 5), and repeated the iRED analysis. The results from this second set of MD trajectories are in good qualitative agreement with the behavior we observed when starting from the most representative conformation: the disappearance of the gap in the collectivity plots at high pressure, and the decrease in the separability index from 3.9 to 3.3 clearly signifies the loss of separability under conditions of high pressure.

A detailed analysis of correlations in the motions of the backbone along different sites on the sequence of ubiquitin reveals the nature and extent of these changes (Fig. 6 *b*). This analysis overcomes the limitations of the generalized order parameter because it measures correlations over all reorientational modes. At high pressure, backbone motions within the N2 conformer become uncorrelated, as illustrated by the disappearance of high-contour regions in the map of correlated dynamics. The loss of cooperativity in the motions of the extended α-helix, residues 23–34, is striking. On the other hand, the N1 population that dominates the ensemble at low-pressure conditions seems to behave similarly under conditions of low and high pressure. Large-amplitude collective motions were observed for residues 23–34 in the extended α-helix, as illustrated in the map of that conformer (Fig. 6 *a*). The high-density contour of this map exactly corresponds to the position of helix residues. A recent study that used residual dipolar coupling (RDC) measurements in a series of alignment media (50) interpreted the model-free derived order parameters and motional anisotropies in terms of cooperative reorientational motion of the helix with respect to the core of the protein. The authors suggested a detailed model of the motions that includes correlated anisotropic exclusions of the α-helix amide bond vectors, with respect to the axis of the helix. Although the timescales inspected with RDCs are longer than those accessible by NMR relaxation experiments and MD simulations (NMR relaxation parameters and MD trajectories probe motions at the ps-ns timescale, whereas RDCs are sensitive to motions at

the ps-ms timescale), our results corroborate the proposed model, in terms of the large-amplitude correlated backbone dynamics of residues along the extended helix, for the N1 conformer. Furthermore, we suggest that this motional mode is absent at high pressure, as indicated by analysis of the iRED covariance matrix of the N2 trajectories under conditions of high pressure. In fact, the lack of correlation in the motions of the α-helix backbone amides for this conformer is evident even under conditions of low pressure, according to the maps of correlated dynamics (Fig. 6 *b*, *upper left quadrant*). Taken together, these results suggest that the dynamics of the extended α-helical region are markedly altered for the N2 population of ubiquitin's ensemble.

At low pressure, the N2 conformer displays increased backbone mobility at its C-terminus, at residues 69–76, compared to the N1 ensemble, according to the iRED-derived generalized order parameters (Fig. 2 *a*). This was also observed experimentally by Kitahara and co-workers (18) in their chemical shift perturbation study that revealed the presence of the two conformers. The authors found that the intensities of the observed NOEs are significantly decreased at high pressure for residues beyond 70. It was proposed in the same study that this happens indirectly, through the destabilization of the backbone hydrogen bonds involving residues 67–72 that participate in the β_5 sheet at the core of the structure. Taken together, these results demonstrate the extent of allosteric effects in the internal dynamics of the molecule: a change in the structure of a core region may affect the dynamics of the structurally distant C-terminus. Given the functional significance of the C-terminus of ubiquitin as a key binding site of several cell factors (reviewed in Ciechanover (51)), this effect may modulate the way ubiquitin recognizes its partners. According to this hypothesis, destabilization of the core strand would increase the mobility of the C-terminus and increase the potential of the N2 conformer to interact with other cellular proteins. In a recent experimental study (52), small changes in the structure of the C-terminal β-sheet induced by mutation of a single residue in the core of the protein were found to be critical for the molecular recognition properties of ubiquitin toward two structurally distinct ubiquitin-binding domains (UBDs): the change abolished binding of ubiquitin-interacting motifs (UIMs), but had no effect on binding of ubiquitin-associated domains (UBAs). These minor structural changes of the β_5 strand were accompanied by changes in the rigidity of the molecule. In light of these results, the implication is that differences in dynamics of the C-terminus for the two conformers are very likely to play a key functional role.

Finally, our analysis indicates that the order parameter based on the model-free fitting of the relaxation data does not adequately account for the high-pressure behavior of the system. The lack of separability between global and internal motions is the main reason for this discrepancy, as indicated in Fig. 1. The model-free approach has been repeatedly reported to be unsuited for disordered parts of proteins, in which internal motions alter the overall shape and therefore the diffusive motions of the peptide (25,26,53). In a recent study of RNase A, it was shown that model-free analysis overestimates order parameters and underestimates internal correlation times, relative to a model that accounts for coupling between the modes of global diffusion of the molecule and internal motions (24). Indeed, the order parameters calculated with iRED for these regions is significantly smaller than the ones derived with a model-free analysis. In addition, as reported by Kitahara and co-workers (19), model-free analysis of the ubiquitin relaxation parameters fails to identify any significant differences in the ps-ns backbone dynamics at high and low pressure. This result seems controversial, given the wide range of chemical shift changes that occur at higher pressure (18), and the extensive differences in the NMR-derived conformers N1 and N2. Our MD-based analysis suggests in extensive detail the changes in dynamics associated with pressure increase, and the transition from the N1-dominated ensemble to the N2-dominated ensemble. Furthermore, the iRED results presented here are validated through direct comparison with the measured NMR relaxation rate constants. Our results are biologically meaningful, since N2 may account for a significant part of the population at physiological pressure (~25% as suggested by chemical shift data (18)). This conformational variability has implications for ubiquitin's function at the ensemble level through the altered dynamics of binding sites for its protein partners, and may provide the means for it to participate in a diverse range of protein-protein interactions.

SUPPLEMENTARY MATERIAL

To view all of the supplemental files associated with this article, visit www.biophysj.org.

We thank Dr. Rafael Bruschweiler for useful discussion on the iRED method, and Dr. K. Akazaka and Dr. R. Kitahara for sharing their NMR data and useful discussions.

The authors acknowledge financial support from Rensselaer Polytechnic Institute and the National Science Foundation (MCB 0543769).

REFERENCES

1. Hershko, A., and A. Ciechanover. 1998. The ubiquitin system. *Annu. Rev. Biochem.* 67:425–479.
2. Groll, M., L. Ditzel, J. Lowe, D. Stock, M. Bochtler, H. D. Bartunik, and R. Huber. 1997. Structure of 20S proteasome from yeast at 2.4 angstrom resolution. *Nature*. 386:463–471.
3. Cornilescu, G., J. L. Marquardt, M. Ottiger, and A. Bax. 1998. Validation of protein structure from anisotropic carbonyl chemical shifts in a dilute liquid crystalline phase. *J. Am. Chem. Soc.* 120:6836–6837.
4. Distefano, D. L., and A. J. Wand. 1987. Two-dimensional H-1-NMR study of human ubiquitin—a main chain directed assignment and structure. *Biochemistry.* 26:7272–7281.
5. Weber, P. L., S. C. Brown, and L. Mueller. 1987. Sequential H-1-NMR assignments and secondary structure identification of human ubiquitin. *Biochemistry.* 26:7282–7290.

6. Vijay-Kumar, S., C. E. Bugg, and W. J. Cook. 1987. Structure of ubiquitin refined at 1.8 a resolution. *J. Mol. Biol.* 194:531–544.
7. Majumdar, A., and R. Ghose. 2004. Probing slow backbone dynamics in proteins using TROSY-based experiments to detect cross-correlated time-modulation of isotropic chemical shifts. *J. Biomol. NMR.* 28:213–227.
8. Lienin, S. F., T. Bremi, B. Brutscher, R. Bruschweiler, and R. R. Ernst. 1998. Anisotropic intramolecular backbone dynamics of ubiquitin characterized by NMR relaxation and MD computer simulation. *J. Am. Chem. Soc.* 120:9870–9879.
9. Tjandra, N., S. E. Feller, R. W. Pastor, and A. Bax. 1995. Rotational diffusion anisotropy of human ubiquitin from N-15 NMR relaxation. *J. Am. Chem. Soc.* 117:12562–12566.
10. Schneider, D. M., M. J. Dellwo, and A. J. Wand. 1992. Fast internal main-chain dynamics of human ubiquitin. *Biochemistry.* 31:3645–3652.
11. Day, R., and A. E. Garcia. 2008. Water penetration in the low and high pressure native states of ubiquitin. *Proteins.* 70:1175–1184.
12. Pan, Y., and M. S. Briggs. 1992. Hydrogen-exchange in native and alcohol forms of ubiquitin. *Biochemistry.* 31:11405–11412.
13. Massi, F., M. J. Grey, and A. G. Palmer. 2005. Microsecond timescale backbone conformational dynamics in ubiquitin studied with NMR R-1p relaxation experiments. *Protein Sci.* 14:735–742.
14. Dittmer, J., and G. Bodenhausen. 2004. Evidence for slow motion in proteins by multiple refocusing of heteronuclear nitrogen/proton multiple quantum coherences in NMR. *J. Am. Chem. Soc.* 126:1314–1315.
15. Wist, J., D. Frueh, J. R. Tolman, and G. Bodenhausen. 2004. Triple quantum decoherence under multiple refocusing: slow correlated chemical shift modulations of C′ and N nuclei in proteins. *J. Biomol. NMR.* 28:263–272.
16. Mills, J. L., and T. Szyperski. 2002. Protein dynamics in supercooled water: the search for slow motional modes. *J. Biomol. NMR.* 23:63–67.
17. Frauenfelder, H., S. G. Sligar, and P. G. Wolynes. 1991. The energy landscapes and motions of proteins. *Science.* 254:1598–1603.
18. Kitahara, R., H. Yamada, and K. Akasaka. 2001. Two folded conformers of ubiquitin revealed by high-pressure NMR. *Biochemistry.* 40:13556–13563.
19. Kitahara, R., S. Yokoyama, and K. Akasaka. 2005. NMR snapshots of a fluctuating protein structure: ubiquitin at 30 bar-3 kbar. *J. Mol. Biol.* 347:277–285.
20. Lipari, G., and A. Szabo. 1982. Model-free approach to the interpretation of nuclear magnetic-resonance relaxation in macromolecules. 1. Theory and range of validity. *J. Am. Chem. Soc.* 104:4546–4559.
21. Bouvignies, G., P. Markwick, R. Bruschweiler, and M. Blackledge. 2006. Simultaneous determination of protein backbone structure and dynamics from residual dipolar couplings. *J. Am. Chem. Soc.* 128:15100–15101.
22. Lipari, G., and A. Szabo. 1982. Model-free approach to the interpretation of nuclear magnetic-resonance relaxation in macromolecules. 2. Analysis of experimental results. *J. Am. Chem. Soc.* 104:4559–4570.
23. Clore, G. M., A. Szabo, A. Bax, L. E. Kay, P. C. Driscoll, and A. M. Gronenborn. 1990. Deviations from the simple 2-parameter model-free approach to the interpretation of N-15 nuclear magnetic-relaxation of proteins. *J. Am. Chem. Soc.* 112:4989–4991.
24. Tugarinov, V., Z. Liang, Y. E. Shapiro, J. H. Freed, and E. Meirovitch. 2001. A structural mode-coupling approach to 15N NMR relaxation in proteins. *J. Am. Chem. Soc.* 123:3055–3063.
25. Bruschweiler, R. 2003. New approaches to the dynamic interpretation and prediction of NMR relaxation data from proteins. *Curr. Opin. Struct. Biol.* 13:175–183.
26. Case, D. A. 2002. Molecular dynamics and NMR spin relaxation in proteins. *Acc. Chem. Res.* 35:325–331.
27. Markwick, P. R., G. Bouvignies, and M. Blackledge. 2007. Exploring multiple timescale motions in protein GB3 using accelerated molecular dynamics and NMR spectroscopy. *J. Am. Chem. Soc.* 129:4724–4730.
28. Prompers, J. J., and R. Bruschweiler. 2002. General framework for studying the dynamics of folded and nonfolded proteins by NMR relaxation spectroscopy and MD simulation. *J. Am. Chem. Soc.* 124:4522–4534.
29. Prompers, J. J., and R. Bruschweiler. 2001. Reorientational eigenmode dynamics: a combined MD/NMR relaxation analysis method for flexible parts in globular proteins. *J. Am. Chem. Soc.* 123:7305–7313.
30. Zhang, F., and R. Bruschweiler. 2002. Contact model for the prediction of NMR N-H order parameters in globular proteins. *J. Am. Chem. Soc.* 124:12654–12655.
31. Wilkinson, K. D., and A. N. Mayer. 1986. Alcohol-induced conformational changes of ubiquitin. *Arch. Biochem. Biophys.* 250:390–399.
32. Showalter, S. A., and K. B. Hall. 2005. Isotropic reorientational eigenmode dynamics complements NMR relaxation measurements for RNA. *In* Nuclear Magnetic Resonance of Biological Macromolecules, Part C. T. L. James, editor. Academic Press, New York. 465–480.
33. Showalter, S. A., and K. B. Hall. 2005. Correlated motions in the U1 snRNA stem/loop 2: U1A RBD1 complex. *Biophys. J.* 89:2046–2058.
34. Musselman, C., H. M. Al-Hashimi, and I. Andricioaei. 2007. iRED analysis of TAR RNA reveals motional coupling, long-range correlations, and a dynamical hinge. *Biophys. J.* 93:411–422.
35. Hummer, G., S. Garde, A. E. Garcia, M. E. Paulaitis, and L. R. Pratt. 1998. The pressure dependence of hydrophobic interactions is consistent with the observed pressure denaturation of proteins. *Proc. Natl. Acad. Sci. USA.* 95:1552–1555.
36. Case, D. A., T. E. Cheatham 3rd, T. Darden, H. Gohlke, R. Luo, K. M. Merz, Jr., A. Onufriev, C. Simmerling, B. Wang, and R. J. Woods. 2005. The Amber biomolecular simulation programs. *J. Comput. Chem.* 26:1668–1688.
37. Van Der Spoel, D., E. Lindahl, B. Hess, G. Groenhof, A. E. Mark, and H. J. Berendsen. 2005. GROMACS: fast, flexible, and free. *J. Comput. Chem.* 26:1701–1718.
38. Cornell, W. D., P. Cieplak, C. I. Bayly, I. R. Gould, K. M. Merz, D. M. Ferguson, D. C. Spellmeyer, T. Fox, J. W. Caldwell, and P. A. Kollman. 1995. A 2nd generation force-field for the simulation of proteins, nucleic-acids, and organic-molecules. *J. Am. Chem. Soc.* 117:5179–5197.
39. Jorgensen, W. L., J. Chandrasekhar, J. D. Madura, R. W. Impey, and M. L. Klein. 1983. Comparison of simple potential functions for simulating liquid water. *J. Chem. Phys.* 79:926–935.
40. Hoover, W. G. 1985. Canonical dynamics—equilibrium phase-space distributions. *Phys. Rev. A.* 31:1695–1697.
41. Nose, S. 1984. A molecular-dynamics method for simulations in the canonical ensemble. *Mol. Phys.* 52:255–268.
42. Parrinello, M., and A. Rahman. 1981. Polymorphic transitions in single-crystals—a new molecular-dynamics method. *J. Appl. Phys.* 52:7182–7190.
43. Darden, T., D. York, and L. Pedersen. 1993. Particle mesh Ewald—an N.Log(N) method for ewald sums in large systems. *J. Chem. Phys.* 98:10089–10092.
44. Fischer, M. W. F., A. Majumdar, and E. R. P. Zuiderweg. 1998. Protein NMR relaxation: theory, applications and outlook. *Prog. Nucl. Magn. Reson. Spectrosc.* 33:207–272.
45. Zwanzig, R., and N. K. Ailawadi. 1969. Statistical error due to finite time averaging in computer experiments. *Phys. Rev.* 182:280–283.
46. Bruschweiler, R. 1992. Normal-modes and NMR order parameters in proteins. *J. Am. Chem. Soc.* 114:5341–5344.
47. Feller, S. E., R. W. Pastor, A. Rojnuckarin, S. Bogusz, and B. R. Brooks. 1996. Effect of electrostatic force truncation on interfacial and transport properties of water. *J. Phys. Chem.* 100:17011–17020.

48. Shen, M. Y., and K. F. Freed. 2002. Long time dynamics of met-enkephalin: comparison of explicit and implicit solvent models. *Biophys. J.* 82:1791–1808.

49. Kay, L. E., D. A. Torchia, and A. Bax. 1989. Backbone dynamics of proteins as studied by 15N inverse detected heteronuclear NMR spectroscopy: application to staphylococcal nuclease. *Biochemistry*. 28:8972–8979.

50. Meiler, J., W. Peti, and C. Griesinger. 2003. Dipolar couplings in multiple alignments suggest alpha helical motion in ubiquitin. *J. Am. Chem. Soc*. 125:8072–8073.

51. Ciechanover, A. 1998. The ubiquitin-proteasome pathway: on protein death and cell life. *EMBO J*. 17:7151–7160.

52. Haririnia, A., R. Verma, N. Purohit, M. Z. Twarog, R. J. Deshaies, D. Bolon, and D. Fushman. 2008. Mutations in the hydrophobic core of ubiquitin differentially affect its recognition by receptor proteins. *J. Mol. Biol*. 375:979–996.

53. Palmer 3rd, A. G. 2004. NMR characterization of the dynamics of biomacromolecules. *Chem. Rev*. 104:3623–3640.